Second-order Raman spectra and lattice dynamics in AlAs

1995 J. Phys.: Condens. Matter 7 1949

(http://iopscience.iop.org/0953-8984/7/9/018)

J. Phys.: Condens. Matter 7 (1995) 1949–1957. Printed in the UK

Second-order Raman spectra and lattice dynamics in AlAs

T Azuhata†, T Sota†‡ and K Suzuki†§

† Department of Electrical Engineering, Waseda University, Shinjuku, Tokyo 169, Japan
‡ Advanced Research Center for Science and Engineering, Waseda University, Shinjuku, Tokyo 169, Japan
§ Kagami Memorial Laboratory for Material Science and Technology, Waseda University, Shinjuku, Tokyo 169, Japan

Received 19 October 1994, in final form 2 December 1994

Abstract. We have re-examined the second-order Raman spectra in a thick AlAs layer grown on a GaAs substrate by polarized Raman spectroscopy. So as to reproduce the spectra, the force constants have been refined and then the phonon dispersion has been calculated within a modified version of the adiabatic bond-charge model. We present phonon frequencies at critical points, e.g. Γ, X, L and W, and the force constants for AlAs. The phonon dispersion is compared with a previous *ab initio* result and it is shown that the procedure presented herein is useful. A brief discussion is also given of the analysis of the second-order Raman spectra of AlSb.

1. Introduction

Information on phonon dispersion is important in considering the electronic conduction, the non-radiative relaxation process of electrons and so on. Inelastic neutron scattering (INS) is a powerful experimental method for investigating phonon dispersion over the whole Brillouin zone. With respect to AlAs, one of the typical III–V compound semiconductors, no INS experiment has been performed, because it is difficult to grow a sufficiently large single crystal of good quality and free from oxidation.

In the early stage of studying the phonon structure in AlAs, several workers have reported phonon frequencies at critical points in the Brillouin zone by various experimental methods, e.g. the analysis of the fundamental absorption edge [1, 2], the photoluminescence excitation method [3] and second-order Raman spectroscopy [4, 5]. After the establishment of molecular beam epitaxy (MBE) as a crystal growth technique, the phonon dispersion of AlAs along the Δ [6–8] and Λ [9, 10] lines has also been obtained using confined optical phonons in GaAs/AlAs superlattices. Quite recently, Spencer *et al* [11] and Wagner *et al* [12] have measured second-order Raman bands in AlAs layers on GaAs substrates grown by MBE and reported the overtone frequencies at the X and L points. Spencer *et al* have also shown that calculated phonon dispersion curves can be tested by the bands.

From a theoretical viewpoint, *ab initio* calculations have been performed on phonon dispersion in both IV and III–V compound semiconductors including AlAs by Giannozzi *et al* [13]. Their results have been used to assign the overtone frequencies in [11, 12]. Although the results for AlAs calculated by Giannozzi *et al* seem to be reasonable, their method requires extensive use of computer time. Thus a realistic lattice-dynamical model still seems to be useful, e.g. in the comparison of experimental and theoretical results for the second-order Raman bands.

In this paper we present results both on the re-examination of the second-order Raman bands in a 1.2 μm AlAs layer grown on a GaAs substrate by MBE and on the phonon

0953-8984/95/091949+09$19.50

dispersion in AlAs calculated using a modified adiabatic bond-charge model (BCM). The second-order Raman bands, whose major component consists of the overtone process, have been measured under the off-resonance condition. The force constants as adjustable parameters used in calculating phonon dispersion have been determined so as to reproduce the experimental results. We have clarified the origin of characteristic structures appearing in the two-phonon density of states. Our calculation has reconfirmed the result of *ab initio* calculations. Brief discussions are also given on the phonon dispersion and the two-phonon density of states for overtones in AlSb.

2. Experiments

The sample used here was grown on a [001]-oriented semi-insulating GaAs substrate by MBE, whose structure is as follows: GaAs(11.9 nm)/AlAs(77.3 nm)/GaAs(11.9 nm)/AlAs(1236.0 nm)/GaAs substrate. The thickness of each layer was determined by the reflection high-energy electron diffraction oscillation. The growth temperature was $T_s = 620\,^{\circ}\mathrm{C}$ and the growth rates were 1 μm h^{-1} for GaAs and 0.8 μm h^{-1} for AlAs. The growth was not interrupted at each interface.

The Raman spectra were recorded in back-scattering geometry at room temperature. The second harmonics ($\lambda_L = 532$ nm) of a quasi-CW Nd^{3+}:YAG laser was used as an exciting light source. The incident laser powers were $I_L \simeq 200$ mW and $I_L \simeq 500$ mW. The scattered light was dispersed by a triple spectrograph of 1.0 m focal length, which consists of a double subtractive filter and a spectrograph stage, and was detected with an image-intensified multichannel detector. To avoid Raman scattering from air in the low-frequency region, the sample was mounted in vacuum.

In figure 1 is shown the Raman spectra measured in the configuration $Z(XX)\bar{Z}$ with the incident laser power $I_L \simeq 200$ mW. The inset in figure 1 shows the high-frequency spectra which have been measured with the somewhat higher laser power $I_L \simeq 500$ mW. The overall features of the spectra are similar to those reported previously [11, 12] except for the bands in the region $\omega \leqslant 100$ cm^{-1}. In the $Z(XX)\bar{Z}$ configuration, first-order scattering is forbidden. Thus the appearance of the 402 cm^{-1} and 360 cm^{-1} peaks is due to the leakage of LO(Γ) and TO(Γ) AlAs phonons, respectively. Similarly, the peaks at 292 cm^{-1} and 268 cm^{-1} are attributed to the leakage of LO(Γ) and TO(Γ) phonon signals from the GaAs substrate. Note that the Raman signals from the upper three layers can be neglected both because of the requirement of the momentum conservation and because the scattering volume is small.

According to group-theoretical considerations in III–V compound semiconductors with the zincblende-type structure, Raman signals due to the two-phonon processes belonging to the irreducible representations $\Gamma_1 + 4\Gamma_{12}$ appear in the $Z(XX)\bar{Z}$ configuration. As is well known, Raman signals belonging to Γ_{12} are negligibly weak in comparison with those belonging to Γ_1, and the dominant parts of signals in Γ_1 come from the overtones. Therefore we regard the major parts of the spectra shown in figure 1 as the overtone spectra.

3. Calculations and results

We have calculated the phonon dispersion of AlAs and the corresponding two-phonon density of states for overtones using a modified version of the adiabatic BCM to analyse the overtone spectra. In the original model for III–V compound semiconductors proposed

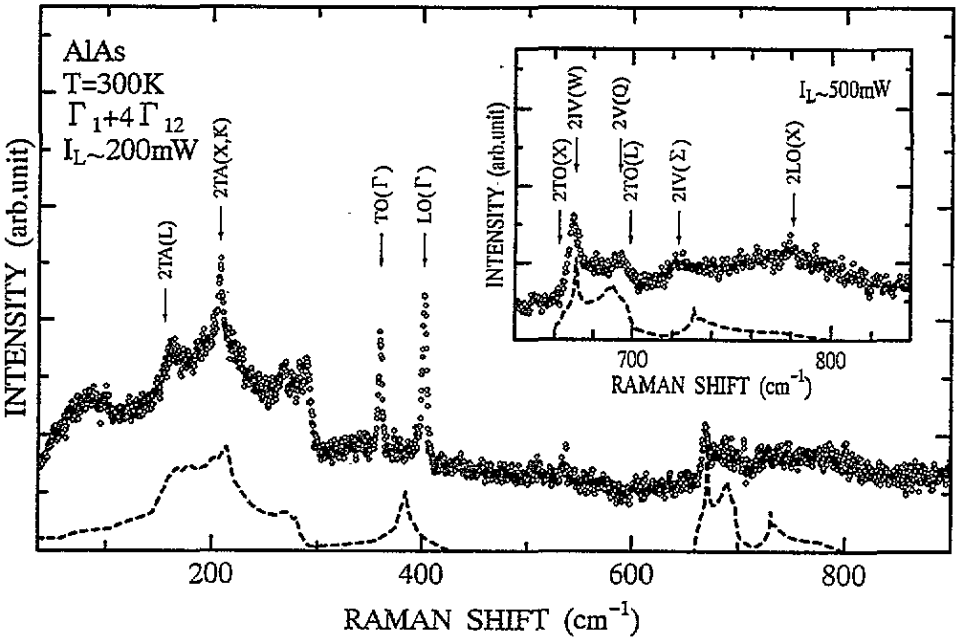

Figure 1. Second-order Raman spectra in a thick AlAs layer at $T = 300$ K with the laser power $I_L \simeq 200$ mW, together with the inset showing the spectra in the higher-frequency region with $I_L \simeq 500$ mW: – – –, two-phonon density of states for overtones calculated using the modified BCM; ↓, characteristic overtone frequencies of phonons at critical points. For the symbols Σ and Q, see text.

by Rustagi and Weber [14], the following was assumed or taken into account. Let the subscripts 1, 2 and BC refer to the metal ion, the non-metal ion and the bond charge (BC). The BC divides the bond length in the ratio 5:3. The two ionic charges are equal, i.e. $Z_1 = Z_2 = -2Z$, where Z is the BC. Coulomb forces acting on the ions and the BCs are calculated by the Ewald method, where the value of Z and the above-mentioned relation are used. The short-range force constants used are the bond-stretching and the bond-bending force constants derived from the central potentials ϕ_{1-2}, ϕ_{1-BC} and ϕ_{2-BC} and from the bond-bending Keating potentials $V_{BC-1-BC}$ and $V_{BC-2-BC}$. The values of ϕ'_{1-2} and ϕ'_{i-BC} with $i = 1, 2$ are determined from the equilibrium condition using the Madelung constant where primes denote the derivatives with respect to the distance. The force constant due to the purely antisymmetric direct BC–BC potential is also taken into account and its value is taken to be $(\beta_1 - \beta_2)/8$ where β_1 and β_2 are the strengths of $V_{BC-1-BC}$ and $V_{BC-2-BC}$, respectively.

In our modified BCM we have added the short-range force constants derived from the central potentials ϕ_{1-1} and ϕ_{2-2} between next-nearest ions but have omitted the force constant due to the purely antisymmetric direct BC–BC potential. For the former, the restriction that $\phi'_{1-1} = -\phi'_{2-2}$ has been introduced from the equilibrium condition. Therefore the model used herein has nine adjustable parameters. As will be shown below, the choice of the above-mentioned force constants leads to better reproduction of the LO–TO splitting.

We have first tried to reproduce the phonon dispersion of GaAs obtained by INS. In figure 2(a) is shown a comparison between our calculated results and the experimental data [15]. The force constants used in calculations are listed in table 1. Figure 2(a) shows

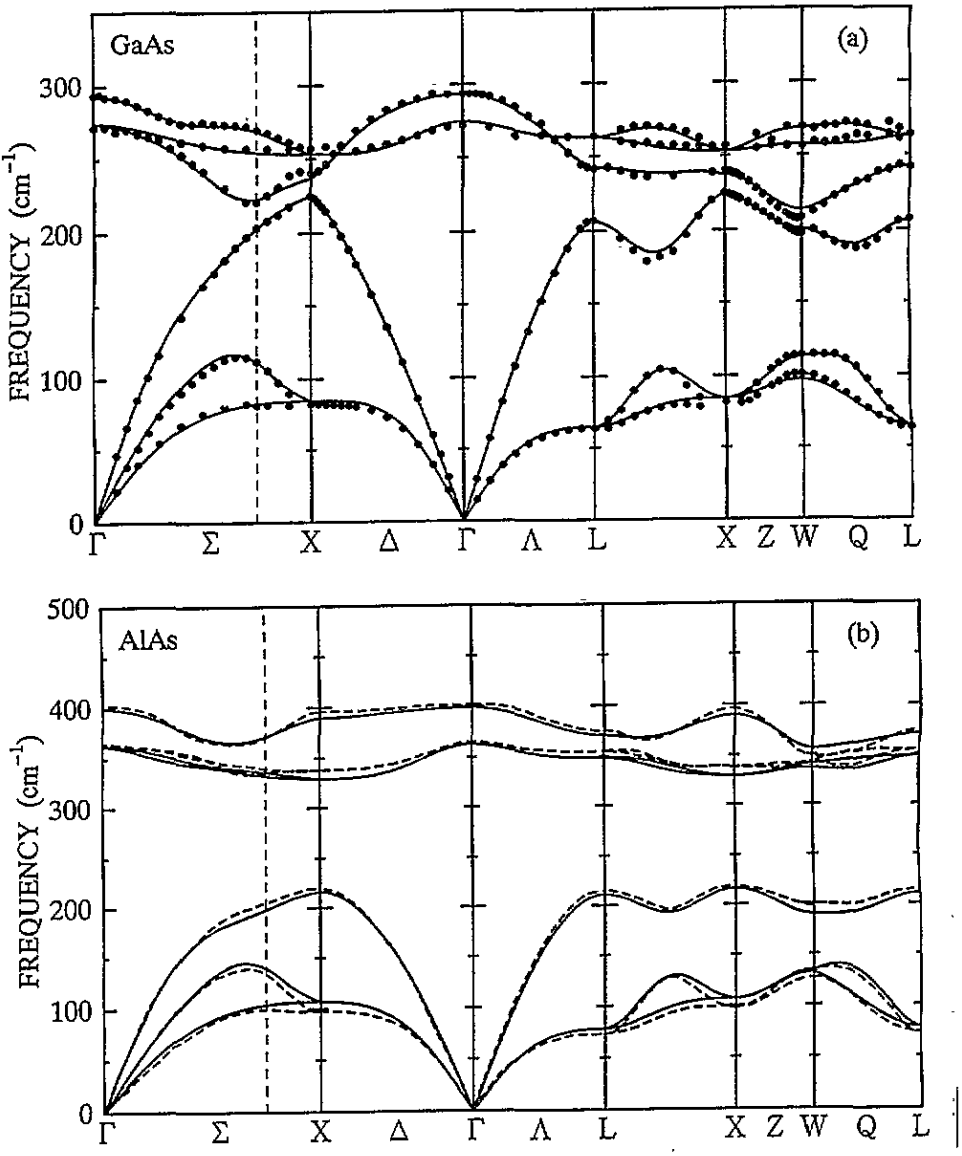

Figure 2. Calculated phonon dispersion curves of (a) GaAs, (b) AlAs and (c) AlSb using the modified BCM (——). For comparison the results of *ab initio* calculations (– – –) (from [13]) are also shown. INS data (●) from [13, 15] are also given. The vertical broken line represents the position of the K point.

satisfactory agreement between the calculation and the experiment. Our modified version of the BCM overcomes the deficiency in the original model that the LO–TO splitting cannot be explained well. The eigenvectors obtained are $e(\mathrm{X}) = 1$ and $e(\mathrm{L}) = 0.875$ according to the representation in [16]. These values are consistent with the experimental results [15, 16], i.e. $e(\mathrm{X}) = 1$ and $e(\mathrm{L}) = 0.58$ or 0.81. Note that the magnitudes of β_1 and β_2 are exchanged in comparison with those reported in [14].

The values of nine parameters for AlAs have been refined to reproduce the second-order Raman spectra through the following procedures. To reproduce them as exactly as possible,

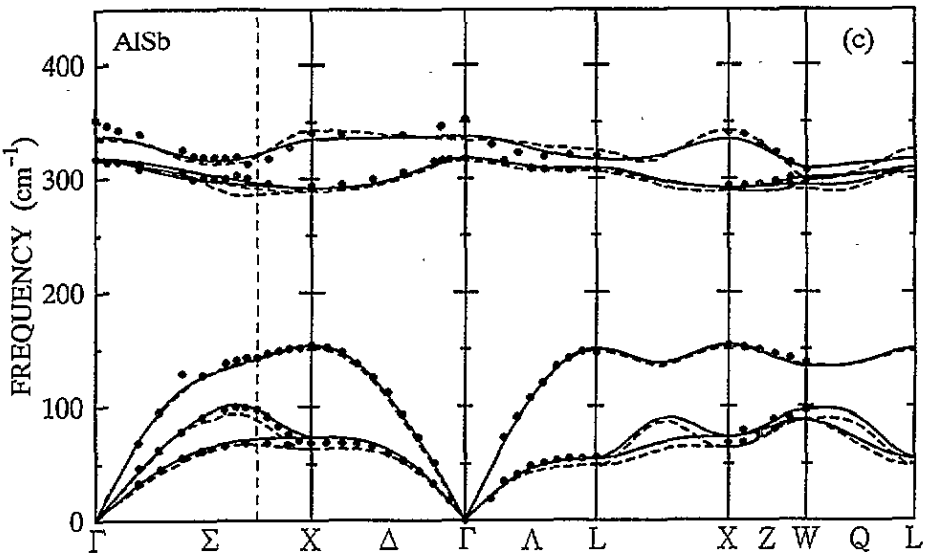

Figure 2. (Continued)

Table 1. Values of force constants refined by using our modified BCM for GaAs, AlAs and AlSb. All values are in units of e^2/v_a. Here v_a is the volume of the unit cell. r_{11} is the distance between the nearest metal ions.

	Ion–ion				Ion–BC		BC–ion–BC		
Material	ϕ''_{1-2}	ϕ''_{1-1}	ϕ''_{2-2}	ϕ'_{1-1}/r_{11}	ϕ''_{1-BC}	ϕ''_{2-BC}	β_1	β_2	Z^2/ε
GaAs	18.467	1.564	−0.342	−0.338	8.215	45.576	6.302	2.484	0.18867
AlAs	19.925	1.093	−0.137	0.246	6.942	47.482	3.869	8.314	0.18790
AlSb	19.633	0.488	0.307	0.347	8.087	46.552	3.676	9.029	0.18955

information is indispensable on phonon frequencies at zone boundary points with high symmetry and/or critical points. However, for AlAs, there exists only a little information from the experiment. To overcome the above-mentioned difficulties, we have first estimated the values of nine parameters for AlAs to reproduce phonon dispersion obtained by *ab initio* calculations [13]. Then, those parameters were refined so as to reproduce the Raman bands.

The best-fit curves obtained for the two-phonon density of states for overtones are shown in figure 1 by broken curves. The temperature factors have been taken into account in the calculation. In figure 1, arrows indicate the characteristic overtone frequencies of phonons at critical points which have been found through the refinement procedures, where the symbols Σ and Q denote the positions with reduced wavevectors $k \simeq (0.65, 0.65, 0)$ and $k \simeq (0.85, 0.5, 0.15)$, respectively. Throughout this paper, we shall use the same notation for phonons as in [15], e.g. IV(Σ) represents the highest-frequency branch along the Σ line. The phonon dispersion obtained is given in figure 2(b) by the solid curves. The broken curves in figure 2(b) represent the results of *ab initio* calculations [13]. The values of nine parameters are listed in table 1. In table 2 we summarize the phonon frequencies at critical points for AlAs. We have obtained the eigenvectors $e(X) = 1$ and $e(L) = 0.993$.

We have also performed the same calculation for AlSb. We have used the second-order Raman bands obtained by Raptis *et al* [17]. The best-fit curves obtained for the

Table 2. Phonon frequencies of AlAs at critical points. The values in the present work are obtained from the second-order Raman spectra and the lattice-dynamical calculations by the modified BCM. For comparison, the results of *ab initio* calculations and the previous experimental data are also shown.

	Phonon frequency (cm^{-1})			
	Previous work		Present work	
Mode	Experiment	*Ab initio* calculation[e]	Theory	Experiment[f]
LO(Γ)	404[a,g],404[b,g]	403	399	402[g]
TO(Γ)	361[a,g],363[b,g]	365	363	360[g]
LO(X)	400[a],396[b],403[c]	396	390	391
TO(X)	340[a],338[b],335[c]	338	329	332
LA(X)	222[c]	219	215	—
TA(X)	103[a],103[b],109[c]	97	107	104
LO(L)	373[d]	375	371	—
TO(L)	350[a],350[b]	354	348	349
LA(L)	—	214	211	—
TA(L)	83[b]	74	78	77
VI(W)	—	348	356	—
V(W)	—	344	341	—
IV(W)	—	344	337	335
III(W)	—	198	190	—
II(W)	—	135	133	—
I(W)	—	127	132	—
IV(Σ)[h]	—	364	365	362
V(Q)[i]	—	351	345	347

[a] [11], $T = 36$ K.
[b] [12], $T = 77$ K.
[c] [3], $T = 4$ K.
[d] [12], $T = 300$ K.
[e] [13].
[f] $T = 300$ K.
[g] From the first-order Raman spectra.
[h] Reduced wavevector $k \simeq (0.65, 0.65, 0)$.
[i] $k \simeq (0.85, 0.5, 0.15)$.

two-phonon density of states for overtones are shown in figure 3 with the experimental data [17], where the symbols Σ, L–X and Q denote the positions with reduced wavevectors $k \simeq (0.65, 0.65, 0)$, $k \simeq (0.75, 0.75, 0.25)$ and $k \simeq (0.85, 0.5, 0.15)$, respectively. The phonon dispersion obtained is given in figure 2(c) together with the results of *ab initio* calculations [13] and the INS data [13]. Fairly good agreement between our calculations and *ab initio* calculations is obtained for AlSb as well as for AlAs. This and the result for GaAs, we believe, justify our model and calculations. Note that the overtone density of states calculated with the modified BCM reproduces the overtone Raman spectra better than that obtained by Raptis *et al* [17] with a valence-overlap shell model. The parameters and the phonon frequencies at critical points for AlSb are listed in tables 1 and 3, respectively. The calculated eigenvectors are $e(X) = 1$ and $e(L) = 0.995$.

4. Discussion

We discuss the correspondence between the second-order Raman bands and the phonon dispersion in AlAs. As can be seen from figure 1, we can divide the frequency region of

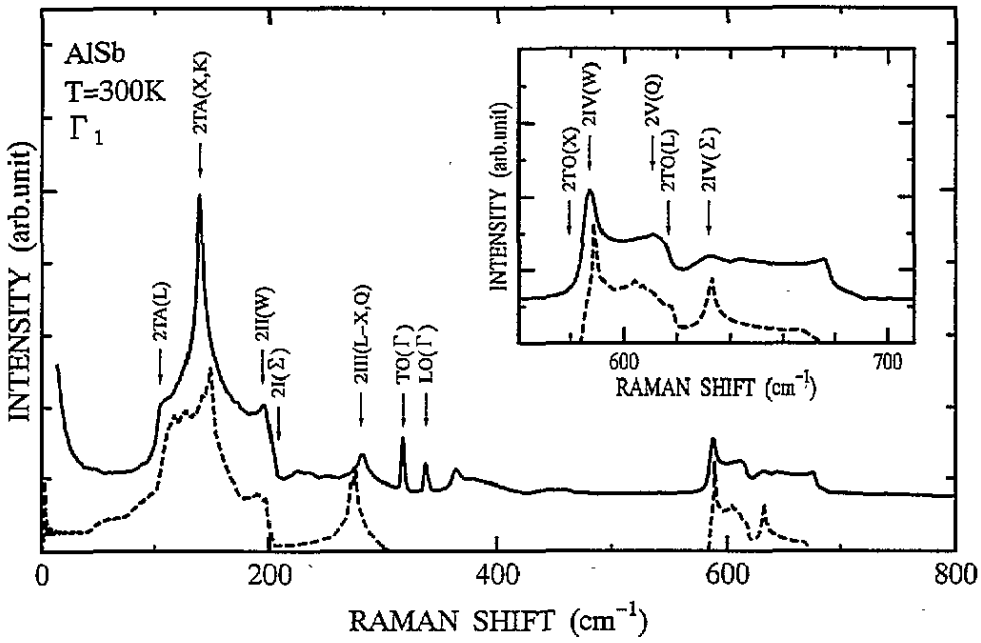

Figure 3. Calculated two-phonon density of states for overtones in AlSb using the modified BCM (– – –): ——, Γ_1 component of the second-order Raman spectra at $T = 300$ K given in [17]; ↓, characteristic overtone frequencies of phonons at critical points. For the symbols Σ, L–X and Q, see text.

the Raman bands into two regions, i.e. $\omega < 450$ cm^{-1} and $\omega > 450$ cm^{-1}. In the former region the bands consist of the overtones arising from the acoustic phonon branches. As indicated by arrows in figure 1, the overtones due to TA(L) and TA(X, K) phonons produce a lower-frequency side edge of peak at 154 cm^{-1} and a peak at 208 cm^{-1}. The increase in the two-phonon density of states near the overtones due to TA(L) and TA(X, K) phonons can be understood from the phonon dispersion of AlAs shown in figure 2(b). With respect to a broad peak centred at 82 cm^{-1}, our calculations show that it belongs to neither the two-phonon density of states of AlAs nor that of GaAs. The origin of the peak may be attributed to disorder-activated transverse acoustic phonons [18]. The bands consisting of the overtones arising from the longitudinal acoustic phonon branches are probably hidden by the leakage of LO(Γ) and TO(Γ) phonons of AlAs.

In the high-frequency region $\omega > 450$ cm^{-1}, the bands consist of the overtones arising from the optical phonon branches. As can be seen from the inset of figure 1, the overtone frequencies due to phonons at the X and L points slightly deviate from the peak positions in the bands. It is found that IV(W), V(Q) and IV(Σ) phonons contribute considerably to the two-phonon density of states. This is also understood from the flat phonon dispersion near those points (see figure 2(b)).

With respect to the second-order Raman bands of AlSb, similar results are obtained (see figure 3 and figure 2(c)). It is worthwhile mentioning that the peak at 280 cm^{-1} in figure 3 is due not to LA(L) but to III(L–X, Q).

As can be seen from tables 2 and 3, we have obtained some new critical frequencies, i.e. IV(W), IV(Σ) and V(Q) for AlAs, and IV(W), II(W), III(L–X), V(Q) and III(Q) for AlSb. Although there are some discrepancies between our experimental frequencies and

Table 3. Phonon frequencies of AlSb at critical points. The values in the present work are obtained from the second-order Raman spectra of [17] and the lattice-dynamical calculations by the modified BCM. For comparison, the results of *ab initio* calculations and the previous experimental data are also shown.

	Phonon frequency (cm^{-1})				
	Previous work			Present work	
Mode	[17][a]	INS[b]	*Ab initio* calculation[c]	Theory	Experiment[d]
LO(Γ)	337[e]	352	334	337	337[e]
TO(Γ)	317[e]	318	316	318	317[e]
LO(X)	338	341	342	335	—
TO(X)	294	294	289	292	290
LA(X)	—	154	152	153	—
TA(X)	65	69	64	74	70
LO(L)	—	320	325	317	—
TO(L)	306	307	306	309	309
LA(L)	142	147	148	150	—
TA(L)	58	56	49	55	53
VI(W)	—	307	298	309	—
V(W)	—	307	298	301	—
IV(W)	—	299	290	294	294
III(W)	—	138	136	135	—
II(W)	—	97	89	97	97
I(W)	—	97	87	89	—
IV(Σ)[f]	316	318	313	316	316
I(Σ)[f]	98	99	94	102	103
III(L–X)[g]	—	—	135	138	140
V(Q)[h]	—	—	302	303	306
III(Q)[h]	—	—	136	135	140

[a] $T = 300$ K.
[b] [13], $T = 15$ K.
[c] [13].
[d] The experimental data in [17] at $T \simeq 300$ K are used.
[e] From the first-order Raman spectra.
[f] Reduced wavevector $k \simeq (0.65, 0.65, 0)$.
[g] $k \simeq (0.75, 0.75, 0.25)$.
[h] $k \simeq (0.85, 0.5, 0.15)$.

our calculated values, it would be possible to decrease them by increasing the number of force constants.

Some discrepancies can be also seen in figures 2(b) and 2(c) between our calculations and *ab initio* calculations at the X and W points and along the Q line. If the *ab initio* calculations give a better result for AlAs, we have to refine our model.

We have calculated the phonon dispersion of material A using the dynamical matrix for material B but the masses of atoms for material A (the so-called mass approximation) for combinations B → A ≡ GaAs → AlAs, AlAs → GaAs, GaAs → AlSb, AlSb → GaAs, AlAs → AlSb and AlSb → AlAs. The matrix has been calculated using the parameters for material B listed in table 1 and the lattice constant of material B. We have compared the dispersion calculated within the mass approximation with the original dispersion. The discrepancy between the former and the latter is at most 13 cm^{-1} for GaAs ↔ AlAs, but more than 30 cm^{-1} for combinations including AlSb. These results are consistent with those obtained by *ab initio* calculations [13] and indicate the validity of our model and parameters.

In summary, we have re-examined the second-order Raman spectra in a thick AlAs layer from both the experiment and the theory. We have obtained the phonon frequencies at several critical points and the values of force constants for AlAs.

Acknowledgment

We are grateful to Mr K Kasahara, NEC Microelectronics Research Laboratories, for supplying the sample.

References

[1] Lorenz M R, Chicotka R, Pettit G D and Dean P J 1970 *Solid State Commun.* **8** 693
[2] Onton A and Chicotka R J 1974 *Phys. Rev.* B **10** 591
[3] Monemar B 1973 *Phys. Rev.* B **8** 5711
[4] Masui H, Klein P B, Chang R K, Callender R H and Chicotka R J 1974 *Proc. 12th Int. Conf. on the Physics of Semiconductors* ed M H Pilkuhn (Stuttgart: Teubner) p 509
[5] Jusserand B and Sapriel J 1981 *Phys. Rev.* B **24** 7194
[6] Wang Z P, Jiang D S and Ploog K 1988 *Solid State Commun.* **65** 661
[7] Pusen Yu A, Milekhin A G, Sinyukov M P, Ploog K and Toropov A I 1990 *JETP Lett.* **52** 464
[8] Mowbray D J, Cardona M and Ploog K 1991 *Phys. Rev.* B **43** 1598
[9] Popović Z V, Cardona M, Richter E, Strauch D, Tapfer L and Ploog K 1990 *Phys. Rev.* B **41** 5904
[10] Calle F, Mowbray D J, Niles D W, Cardona M, Calleja J M and Ploog K 1991 *Phys. Rev.* B **43** 9152
[11] Spencer G S, Grant J, Gray R, Zolman J, Menéndez J, Droopad R and Maracas G N 1994 *Phys. Rev.* B **49** 5761
[12] Wagner J, Fischer A, Braun W and Ploog K 1994 *Phys. Rev.* B **49** 7295
[13] Giannozzi P, de Gironcoli S, Pavone P and Baroni S 1991 *Phys. Rev.* B **43** 7231
For the INS data of AlSb see also Strauch D, Dorner B and Karch K 1990 *Proc. 3rd Int. Conf. on Phonon Physics* ed S Hunklinger, W Ludwig and G Weiss (Singapore: World Scientific) p 82
[14] Rustagi K C and Weber W 1976 *Solid State Commun.* **18** 673
[15] Strauch D and Dorner B 1990 *J. Phys.: Condens. Matter* **2** 1457
[16] Strauch D and Dorner B 1986 *J. Phys. C: Solid State Phys.* **19** 2853
[17] Raptis Y S, Anastassakis E and Kanellis G 1992 *Phys. Rev.* B **46** 15 801
[18] Carles R, Saint-Cricq N, Renucci J B, Renucci M A and Zwick A 1980 *Phys. Rev.* B **22** 4804